International Journal of Greenhouse Gas Control 11S (2012) S35–S46

Contents lists available at SciVerse ScienceDirect

International Journal of Greenhouse Gas Control

journal homepage: www.elsevier.com/locate/ijggc

# Monitoring $CO_2$ storage using ghost reflections retrieved from seismic interferometry

D. Draganov*, K. Heller, R. Ghose

*Department of Geotechnology, Delft University of Technology, Stevinweg 1, 2628 CN, Delft, The Netherlands*

ARTICLE INFO

*Article history:*
Received 7 March 2012
Received in revised form 26 July 2012
Accepted 30 July 2012
Available online 17 August 2012

*Keywords:*
Seismics
$CO_2$
CCS
Monitoring
Reflections
Interferometry
Ultrasonic

ABSTRACT

Time-lapse seismic monitoring constitutes the foundation for most monitoring programmes involving $CO_2$ storage. Two major sources of uncertainty in the estimation of changes in the reservoir properties like saturation and pressure, using time-lapse seismics, are the non-repeatability of the source positions and the difficulty to separate the effect of the overburden from that of the changes taking place in a $CO_2$ reservoir. In order to address those challenges, we propose a new concept of using non-physical (ghost) reflection events retrieved by seismic interferometry. We test this concept on data of realistic numerical modelling and scaled laboratory experiments, both representing a horizontally layered subsurface. Our results demonstrate that the seismic reflection ghosts can indeed be used advantageously to monitor changes in the $CO_2$ reservoir.



## 1. Introduction

Seismic interferometry (SI) is a method that retrieves new seismic traces from the cross-correlation of existing traces. The idea was first proposed for exploration purposes by Claerbout (1968) who showed that the reflection response of a 1D medium can be obtained from the autocorrelation of the transmission response. Later, he conjectured that for a 3D medium, the reflection response could be retrieved from cross-correlation of observed seismic noise. The method gained new momentum at the beginning of this century when several researchers showed how the seismic impulse response (Green's function) between receivers can be extracted from the cross-correlation of measurements at these receivers from transient or noise sources (e.g. Schuster, 2001; Wapenaar et al., 2002; Campillo and Paul, 2003; Shapiro and Campillo, 2004). An extensive overview of the different types of SI and their applications can be found in Wapenaar et al. (2008) and Schuster (2009).

To retrieve the acoustic Green's function $G(\mathbf{x}_B, \mathbf{x}_A, t)$ and its time-reversed variant at $\mathbf{x}_B$ as if from a virtual source at $\mathbf{x}_A$, from observations at the two receivers at $\mathbf{x}_A$ and $\mathbf{x}_B$ at the surface, Wapenaar and Fokkema (2006) showed that one should cross-correlate the observed wavefields at these two points generated by monopole sources at points $\mathbf{x}$ in the subsurface along a source boundary $\partial\mathbb{D}$ (see Fig. 1):

$$G(\mathbf{x}_B, \mathbf{x}_A, t) + G(\mathbf{x}_A, \mathbf{x}_B, -t) \approx \frac{2}{\rho c} \oint_{\partial\mathbb{D}} G(\mathbf{x}_B, \mathbf{x}, t) * G(\mathbf{x}_A, \mathbf{x}, -t)\, d^2\mathbf{x}. \quad (1)$$

In the above equation, $c$ and $\rho$ are, respectively, the constant propagation velocity and mass density at and outside the source boundary $\partial\mathbb{D}$ and $*$ denotes convolution. In the derivation process it has been assumed that there is no intrinsic attenuation in the medium, that $\partial\mathbb{D}$ is a half-sphere with a sufficiently large radius, and that the medium outside $\partial\mathbb{D}$ is homogeneous. When these assumptions are complied with, the application of SI with Eq. (1) for the retrieval of the complete Green's function is straight forward and does not require preprocessing of the recorded responses from the subsurface sources. A reflection arrival between the points $\mathbf{x}_A$ and $\mathbf{x}_B$ (the thick blue lines in Fig. 1) is retrieved by SI from the correlation at these two points of arrivals from subsurface sources laying in the stationary-phase region for this specific reflection (Snieder, 2004), i.e., from sources at $\partial\mathbb{D}$ at and around the specular ray (the thin blue line) that connects $\mathbf{x}_B$ to $\mathbf{x}_A$ through the reflector following Snell's law. The stationary-phase region, illustratively outlined in Fig. 1 by the blue ellipse, lies around the position of the stationary source (the blue star) and its width depends on the distance to the receivers, the medium velocity and the dominant frequency of the source signals. The stationary source lies at the intersection of the

* Corresponding author.
*E-mail addresses:* d.s.draganov@tudelft.nl (D. Draganov), h.k.j.heller@tudelft.nl (K. Heller), r.ghose@tudelft.nl (R. Ghose).

1750-5836/$ – see front matter © 2012 Elsevier Ltd. All rights reserved.
http://dx.doi.org/10.1016/j.ijggc.2012.07.026

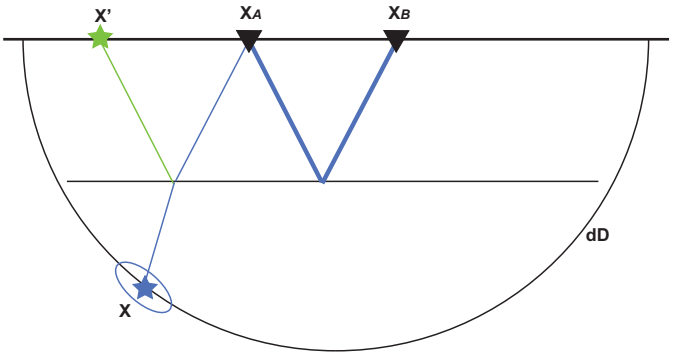


**Fig. 1.** A medium with two receivers (the triangles) at the surface at points $\mathbf{x}_A$ and $\mathbf{x}_B$. To retrieve the Green's function between the receivers, one needs to cross-correlate the seismic response from sources along the source boundary $\partial\mathbb{D}$ (one shown here at point $\mathbf{x}$). The coloured lines indicate seismic rays; the blue ellipse indicates the stationary-phase region, while the stars represent sources at stationary points. The thick black line illustrates the Earth's surface, which is a free surface for seismic waves.

source boundary with the specular ray through $\mathbf{x}_A$. The correlation and summation process in Eq. (1) retrieves the desired reflection from the direct arrival at $\mathbf{x}_A$ and the reflected arrival at $\mathbf{x}_B$. The correlation process eliminates the common travel path – the thin blue line, while the summation process "picks" the subsurface sources in the stationary-phase region and adds them constructively to leave the retrieved reflection at $\mathbf{x}_B$ due to a virtual source at $\mathbf{x}_A$.

The seismic reflection method has been found effective for monitoring $CO_2$ sequestration in subsurface porous layers (e.g. Arts et al., 2002; Chadwick et al., 2010; Lumley, 2010; Ivanova et al., in press). The time-lapse changes in the seismic velocity are attributable to a combined effect of changes in $CO_2$ saturation and pore pressure in the reservoir. An uncertainty in the estimation of these reservoir parameters through seismic monitoring, though, arises from the non-repeatability of the exact positions of the sources and the receivers at the surface, for example, in marine seismics due to the towed geometry of the surveys. Obtaining virtual sources at the locations of the seismic receivers for the application of Eq. (1) brings the advantage that the uncertainty in the position of the sources is eliminated. This can be especially advantageous when the receivers are at fixed positions at the bottom of the sea. A second challenge, due to the difficulty of separating the effects of the overburden (including the near-surface effects) from changes in the reservoir parameters, can also be addressed by seismic interferometry, especially when using non-physical (ghost) arrivals. The latter arrivals represent energy from virtual sources and receivers redatumed onto the subsurface layer interfaces and can be used to obtain accurate layer-specific properties of subsurface structures, for example directly on the $CO_2$ reservoir. In the following, we explain how the ghosts appear in the SI results and present results to illustrate our idea of using ghost seismic reflections to monitor changes in the $CO_2$ reservoir.

## 2. Idea and method

In a normal seismic survey, the employed sources are not in the subsurface, but at the surface. SI Eq. (1), however, requires the sources to be located in the subsurface. Nevertheless, using stationary-phase arguments, it can be shown that also a source at the Earth's surface can be used (the green star in Fig. 1) when this source lies along the continuation of the specular ray after the energy has reflected from a subsurface reflector (the green line in Fig. 1). In this manner, for all subsurface sources along $\partial\mathbb{D}$, equivalent surface sources can be found. These equivalent sources are a substitute for the subsurface sources present in Eq. (1). This means that to retrieve the desired reflection, one has to correlate a reflected arrival at $\mathbf{x}_A$ with another reflected arrival, in fact a multiple of the first one, at $\mathbf{x}_B$ (van Wijk, 2006). The correlation process again eliminates the common travel path – the thin green and blue lines in Fig. 1 – and leaves the retrieved reflection at $\mathbf{x}_B$ due to a virtual source at $\mathbf{x}_A$.

Using sources only at the Earth's surface, however, comes at a price. Eq. (1) requires that the source surface surrounds the two receivers. When part of this boundary is a free surface, like the Earth's surface, then only sources in the subsurface are required, because the free surface serves as a mirror and, through reflection, turns the half-sphere into a full sphere. In contrast, when using sources only at the surface, no mirror is present and the so-called one-sided illumination of the receivers occurs (Wapenaar, 2006). A consequence of the one-sided illumination is that application of Eq. (1) will retrieve not only the desired physical reflections, but also non-physical (ghost) arrivals. An example of non-physical arrivals are the so-called virtual refractions (e.g. Dong et al., 2006; Tatanova et al., 2008; Mikesell et al., 2009; Bharadwaj et al., 2011). These non-physical events can be identified, as they pass through the virtual-source position at 0 s and have a linear moveout. They can be used to estimate the propagation velocity of P- or S-waves of subsurface layers, for example where the standard refraction method cannot be used (Nichols et al., 2011; Tatanova et al., 2011). Another example of non-physical arrivals are the spurious (peg-leg) multiples as described by Snieder et al. (2006), which represent reflection energy. King et al. (2011) showed that these ghosts can be used in velocity-analysis processing to obtain a better estimate of the subsurface velocities. Draganov et al. (2010) illustrated the possibility of estimating layer-specific seismic attenuation using the ghost reflections from SI. King and Curtis (2012) showed that in marine surveys with towed sources and streamers the spurious multiples can be identified. For this purpose, the authors compared the results retrieved using SI by cross-correlation with the results retrieved using another SI technique, namely source-receiver interferometry (see Curtis, 2010 for explanation of this technique). King and Curtis (2012) also showed that the identified ghost reflections can be used to estimate the layer-specific propagation velocities for the first few layers in the subsurface.

Fig. 2(a) illustrates how ghost reflections are created by the cross-correlation and summation processes from the application of relation (1) to recordings from sources at the surface. A correlation of the reflection arrival at $\mathbf{x}_A$, which has propagated along path 1-2-3-4, with the reflection arrival at $\mathbf{x}_B$, which has propagated along path 1-2-5-6-7-8, eliminates the common travel paths – 1-2-3-4 and 1-2-7-8, respectively. After a constructive summation of the correlated arrivals from sources in the stationary-phase region an arrival is retrieved, which has effectively traversed only the path 5-6. This arrival is, thus, kinematically equivalent to a reflected arrival as if measured with a virtual source and receiver directly placed at the boundary between the second (cap rock) and the third (reservoir) layer. We define such sources and receivers to be ghost sources and receivers. As the medium is assumed here to consist of horizontal layers, the distance between the ghost virtual source and receiver is equal to the distance between the virtual source and receiver at the surface. In a more practical case, when the subsurface is not horizontally layered, the distance between the ghost source and receiver is not equal to the one between the virtual source and receiver at the surface. If a subsurface model is known, though, then this distance can be estimated using ray tracing. The accuracy of the known velocities influences the accuracy of the estimation of the distance between the ghost source and receiver.

The use of retrieved reflection ghosts allows for monitoring changes in the subsurface, such as those caused by injection of $CO_2$ in the reservoir layer. The idea is to perform seismic monitoring in

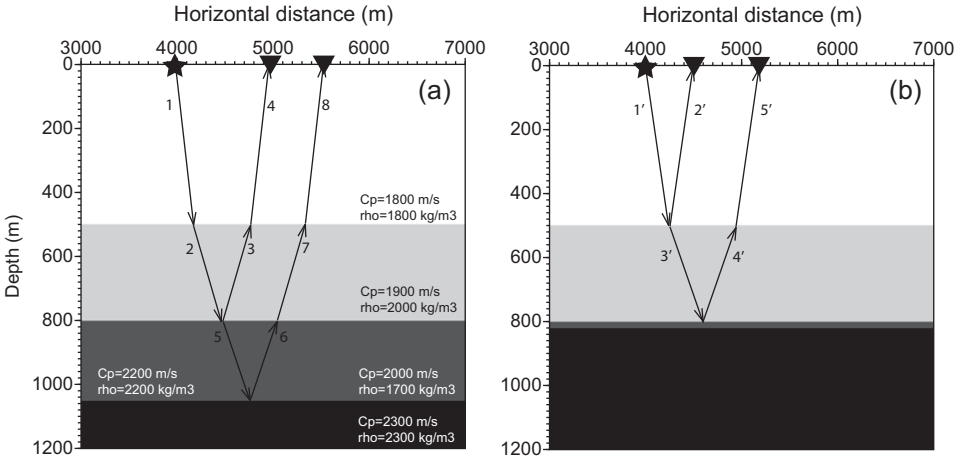


**Fig. 2.** Acoustic subsurface models used to test the idea of monitoring of velocity changes in a $CO_2$ reservoir using SI reflection ghosts. The models consist of horizontal layers with laterally homogeneous propagation velocity and density. The values are indicated in (a) for a thick third (reservoir) layer, derived from the model in Carcione et al. (2006). The raypaths labelled 1-2-3-4 and 1-2-5-6-7-8 illustrate reflections from the top and the bottom of the third layer, respectively. (b) The same model, but for a thin reservoir layer (1/10 of the dominant wavelength). The raypaths labelled 1′-2′ and 1′-3′-4′-5′ illustrate reflections from the top and the bottom of the second (cap rock) layer, respectively. The velocity and density values in the reservoir are changed between the base (values on the left) and the monitor (values on the right) surveys.

a (horizontally) layered subsurface in the following way. Data from a base survey, before injection of $CO_2$, is used in SI to retrieve the virtual reflection results. As the sources in the survey are only at the surface, the retrieved reflection results will contain also reflection ghosts. The standard seismic processing of the base survey results in the identification of the reflection arrivals from the cap rock and the reservoir. The travel-time difference between these two arrivals can be used to identify which ghost reflection corresponds to the reflection from inside the reservoir. Similar identifications can be performed for other ghost reflections, for example from inside the cap rock. Once the monitor survey (after injection of $CO_2$) is concluded, the data from it is again used in SI to retrieve reflection results from virtual sources at the receiver positions. If there was a change in the reservoir or in the cap rock, the retrieved ghost reflections will indicate that directly for each of these layers, as they will have different arrival times than for the base survey. The advantage of using ghost reflections is that they indicate layer-specific changes in the velocity. In the next section we illustrate the proposed workflow of our idea using numerical-modelling and laboratory results.

## 3. Results

In this section, we use first data from numerical modelling to demonstrate how the ghost reflections can be used in monitoring of $CO_2$ sequestration. We then test the applicability of the method on a scaled laboratory sample using high-frequency P-waves.

### 3.1. Numerical results

We use a finite-difference modelling code (Thorbecke and Draganov, 2011) in an acoustic mode to generate a seismic reflection dataset. A horizontally layered subsurface model is considered, as shown in Fig. 2. The model in Fig. 2(a), which is derived from the model of Carcione et al. (2006), is representative of the Sleipner field in the North Sea (Arts et al., 2004). In this field, $CO_2$ is being stored inside the Utsira formation; this is a highly permeable porous sandstone lying 800 m below the sea bottom. For the subsurface layers we use the same parameters as in Carcione et al. (2006, Table 3). We consider impulsive sources and receivers placed 1 m below the surface. The sources are placed from 2000 m till 4400 m with a spacing of 20 m. The receivers are placed from 4500 m till 5500 m every 10 m. Note that we do not include the shallow water layer during the modelling, emulating a reflection dataset after application of the water-bottom multiple elimination. As illustrated in Fig. 2(a), we first model a base survey, with P-wave velocity and density in the Utsira layer as 2200 m/s and 2200 kg/m$^3$, and a monitor survey after changing the velocity and density in the same layer to 2000 m/s and 1700 kg/m$^3$, respectively. The mentioned values have been adapted from the observed velocities as provided by Arts et al. (2004).

Fig. 3(a) shows the retrieved reflection gather for a virtual source at 4500 m. This result is obtained by applying SI Eq. (1) to the modelled reflection gathers. Eq. (1) states that when the boundary sources effectively surround the receivers, both the Green's function and its time-reversed version will be obtained. In our case, the surface sources are only to the left side of the receivers. From stationary-phase argument (Snieder, 2004) it follows that for a virtual source at 4500 m, that is at the first receiver position, the time-reversed Green's function will not be retrieved for the case of our subsurface model. For this reason, we take only the positive part of the SI result. Comparing the virtual gather with a directly modelled gather in Fig. 3(b), obtained after using directly an actual source at 4500 m, we can see that SI has retrieved correctly the kinematics of the reflected arrivals from the three layers, except for offsets shorter than 100 m. Incorrect retrieval of offsets for receiver closer to the virtual source than 100 m happens because the active surface source closest to the virtual-source position at 4500 m has an offset of 100 m from it. Why this is the case can be understood using the explanation given in the previous section regarding the retrieval of reflections in Fig. 1 (see also the explanation in King and Curtis (2012)). To retrieve a reflection arrival using SI at a receiver located at 100 m distance from the virtual-source position, for the case of a horizontally layered medium an active surface source is needed at a mirrored position from the receiver relative to the virtual source, which is also located at 100 m from the virtual source. To retrieve correctly the reflected arrivals at offsets shorter than 100 m, the active sources at the surface should also be at distances less than 100 m from the virtual source. We do not model this situation, as in a marine survey the shortest offsets are not present. Note that the wavelets in the retrieved and the directly modelled results are different, as during the retrieval process the correlation produces a virtual-source wavelet that is the autocorrelation of the wavelet of the actual surface sources. If the subsurface is not horizontally layered, the stationary-source position can be estimated by ray tracing.

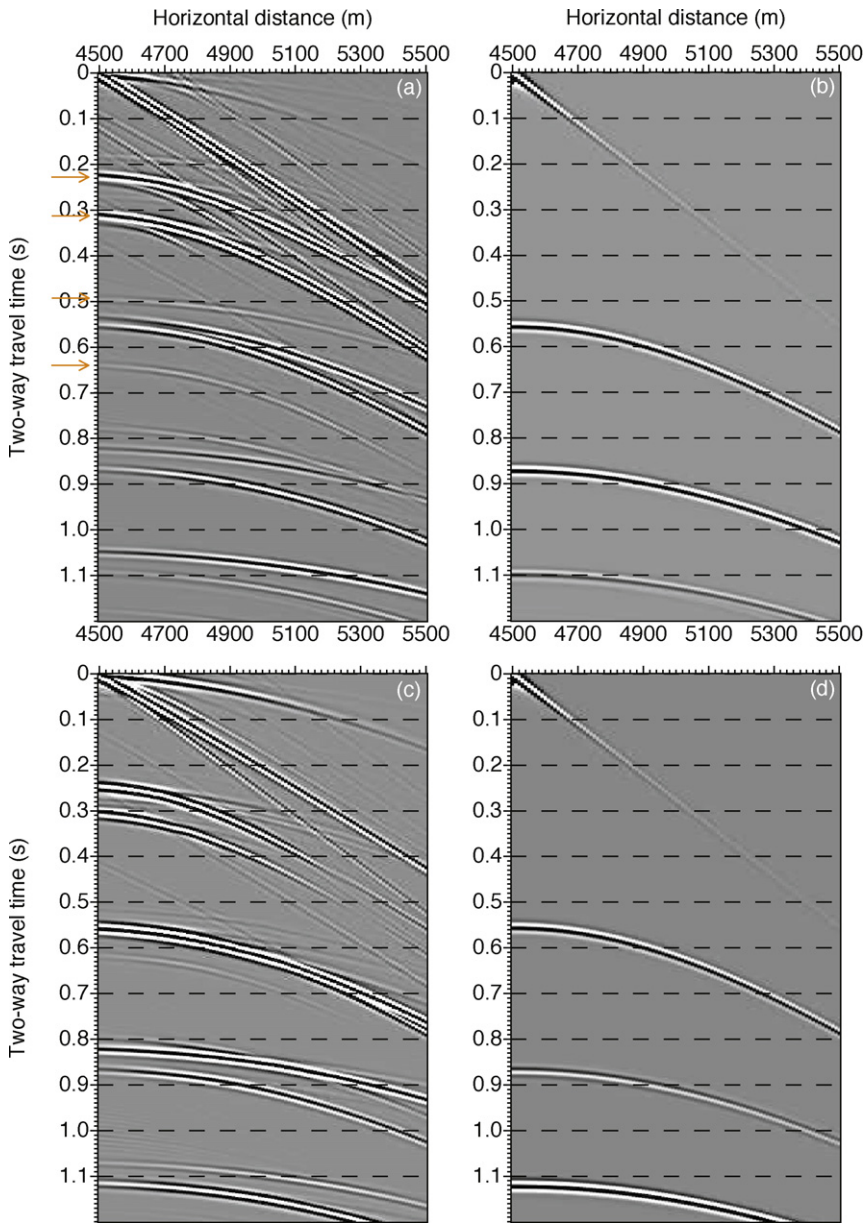


**Fig. 3.** Common-source reflection gathers for the model in Fig. 2(a) for a source at 4500 m. (a) Result retrieved using seismic interferometry for the base survey. The orange arrows indicate examples of ghost arrivals. (b) Directly modelled result for an actual source at 4500 m for the base survey. (c) As in (a), but for the monitor survey. (d) As in (b), but for the monitor survey. For visualization purposes, the amplitudes in each panel are scaled with respect to the maximum amplitude in each panel.

Apart from the physical reflections, the retrieved result in Fig. 3(a) exhibits a score of ghost reflections, like the ones indicated by the orange arrows, that are not present in Fig. 3(b). These events can be interpreted based on information about the thickness of and propagation velocities in the subsurface. Alternatively, the interpretation could be achieved using estimates of the arrival-time differences between different interpreted reflection arrivals. As we use here a numerical model, we know the velocities and thicknesses of the subsurface layers exactly, so we use them for the interpretation. The ghost arrival with an apex at around 0.23 s represents an internal multiple from inside the reservoir layer from ghost source and receiver placed directly on top of the reservoir layer. The ghost reflection with an apex at around 0.32 s is the ghost reflection from inside the cap-rock layer. The ghost arrival with an apex at around 0.49 s represents the multiple of the ghost reflection at 0.23 s; the ghost at 0.54 s represents a reflection between the top of the cap rock and the bottom of the reservoir layer, that is a reflection that has travelled both the cap-rock and the reservoir layers; the ghost at 0.64 s represents the multiple of the ghost reflection at 0.32 s, etc. As explained in the previous section, the ghost reflections at 0.23 s and 0.32 s depend only on the propagation velocity of the seismic waves inside the reservoir and the cap-rock layers, respectively. Any velocity changes inside these layers, due to injection of $CO_2$ in the reservoir or leakage of $CO_2$ to the cap rock for example, should show up as layer-specific changes in the arrival times of the ghost reflections. To make use of the ghosts, though, one should identify them as such and relate them to a specific layer. As explained in the previous section, this is possible using the interpretation results from the normal seismic survey. For example, from the normal processing of the seismic survey, the arrival times of the reflections from the bottom of the cap rock and the reservoir will be interpreted and their difference will give the arrival time of the ghost reflection from inside the reservoir.

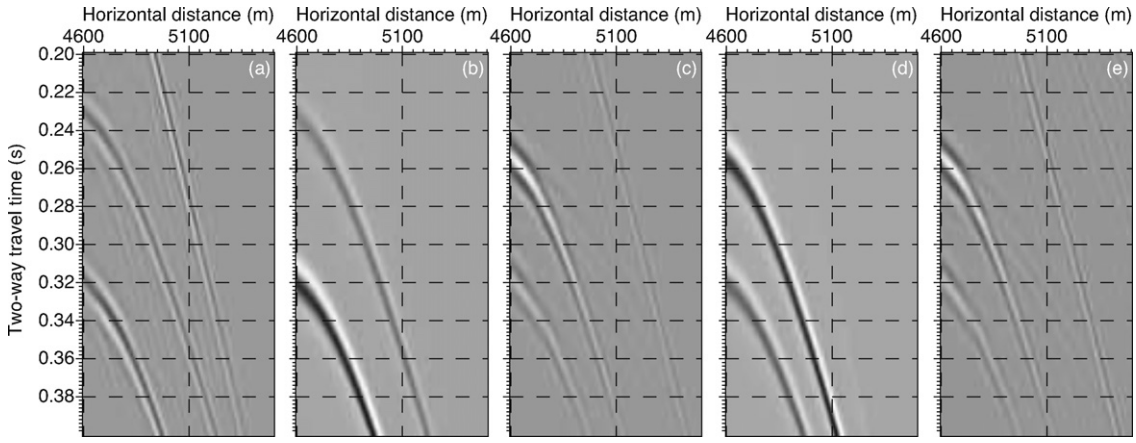


**Fig. 4.** Zoomed-in section of the common-source gathers showing reflections from inside the cap-rock and reservoir layers for the model in Fig. 2(a). (a) Result retrieved using seismic interferometry for the base survey. (b) Directly modelled result for an actual source at the position of the ghost source for the base survey. (c) As in (a), but for the monitor survey. (d) As in (b), but for the monitor survey. (e) As in (c), but when the surface sources have a random non-repeatability of 5 m, 10 m, or 15 m around the respective source positions in the base survey. No scaling has been applied to the amplitudes in these panels.

We apply SI also to the modelled reflection data from the monitor survey (see Fig. 2(a)). The obtained common-source gather for a virtual source at 4500 m is shown in Fig. 3(c) and is compared with the directly modelled common-source gather in Fig. 3(d). Concentrating on the retrieved ghost reflections from inside the reservoir and the cap rock (Fig. 4(a, c)), we can see that the ghost reflection from inside the cap rock does not show changes in its arrival time, while the ghost reflection from inside the reservoir does, as expected from the model used for the monitor survey. In Fig. 4(b, d) we show for comparison the zoomed-in sections around the directly modelled reflections from inside the reservoir and the cap rock for actual sources and receivers placed on top of each of the two layers, for the model parameters of the base and the monitor surveys. Note that the kinematics of the ghost reflections are retrieved correctly, except for the shortest offsets, due that the shortest source-receiver offsets are missing. Assuming that the subsurface is horizontally layered, the offsets from which the ghost reflections are correctly obtained can be calculated.

A common problem in time-lapse seismic monitoring is the non-repeatability of the source and receiver positions. SI has the potential to eliminate errors in the source positions during the monitor survey if the receiver positions are repeatable. To investigate the influence of source position non-repeatability on the retrieved ghost reflections, we model a monitor survey, in which each source position has a random error of 5 m, 10 m or 15 m relative to the respective position in the base survey. Fig. 4(e) shows the retrieved ghost reflections for these surface-source positioning errors. Apart from some weak extra correlation noise, the ghost reflections are at their correct times and with correct moveout. This shows that source non-repeatability does not affect the retrieval of the ghost reflections as long as there are enough surface sources in the stationary-phase regions of each ghost reflection. This is especially advantageous when a permanent receiver network is used at the sea bottom. In such a case, if we were to model step-wise changes in the migration of the injected $CO_2$ (thus introducing lateral inhomogeneity inside the reservoir) and acquire monitor data after each step change, monitoring the $CO_2$-front migration can be performed using common-offset gathers. The SI retrieved ghost reflections will eliminate the non-repeatability in the source positions and allow better resolution in following the $CO_2$-front migration when compared to common-offset gathers from the standard seismic surveys. An extra advantage of a permanent receiver network at the sea bottom is that the ghost reflections will have also their nearest offsets retrieved correctly. Note that, as long as the medium above the reservoir is still laterally homogeneous, even when lateral inhomogeneity inside the reservoir is introduced, the distance between the ghost source and receivers will still be equal to the distance between he respective virtual source and receiver at the surface. Furthermore, obtaining virtual common-source gathers at each receiver position, as possible by the used source-receiver geometry of the marine survey, permits interactive velocity analysis of the retrieved virtual gathers (King and Curtis, 2012). As the medium above the reservoir is horizontally layered, the positions of the ghost source and receivers at the top of the cap rock and the reservoir can be precisely calculated from the surface source-receiver geometry. This would allow estimation of the partial changes in the propagation velocity inside the reservoir layer. When the layers above the reservoir also have lateral changes in their seismic parameters, the ghost reflections can still be retrieved, but the positions of the ghost source and receivers can be estimated only approximately. Still, the ghost reflections can be used for monitoring changes in the reservoir and/or the cap rock, but we would not be able to say in which parts of these layers exactly these changes have taken place (King and Curtis, 2012).

The method we propose for monitoring changes in the reservoirs can also be applied to thin reservoirs. To demonstrate this, we calculate a synthetic seismic dataset for a base and a monitor survey for the model shown in Fig. 2(b), which represents a horizontally layered subsurface with a reservoir layer with a thickness of 1/10 of the dominant wavelength in it. The common-source gathers obtained from SI for a virtual source at 4500 m are shown in Fig. 5(a, c) for the base and the monitor survey, respectively. Comparing these gathers to the ones in Fig. 5(b, d), respectively, obtained from direct modelling with an actual source at 4500 m, we can see that the kinematics of the physical reflections are again correctly retrieved. We can also see a retrieved ghost reflection with an apex at around 0.32 s. Just as in the case of the thick-reservoir model, this ghost reflection corresponds to a reflection as if measured with ghost source and receivers placed directly on top of the cap-rock layer. In this case, though, this is not simply a reflection from inside the cap rock.

Due to the very small thickness of the reservoir we observe the tuning effect (Kallweit and Wood, 1982) – the reflection from the reservoir interferes with the reflection from the bottom of the cap rock to produce a single arrival with a wider wavelet. On application of SI, the correlation of the arrival with raypath 1′-2′ in Fig. 2(b) with the arrival with raypath 1′-3′-4′-5′, we can retrieve the cap-rock ghost reflection that exhibits a wider wavelet (compare the

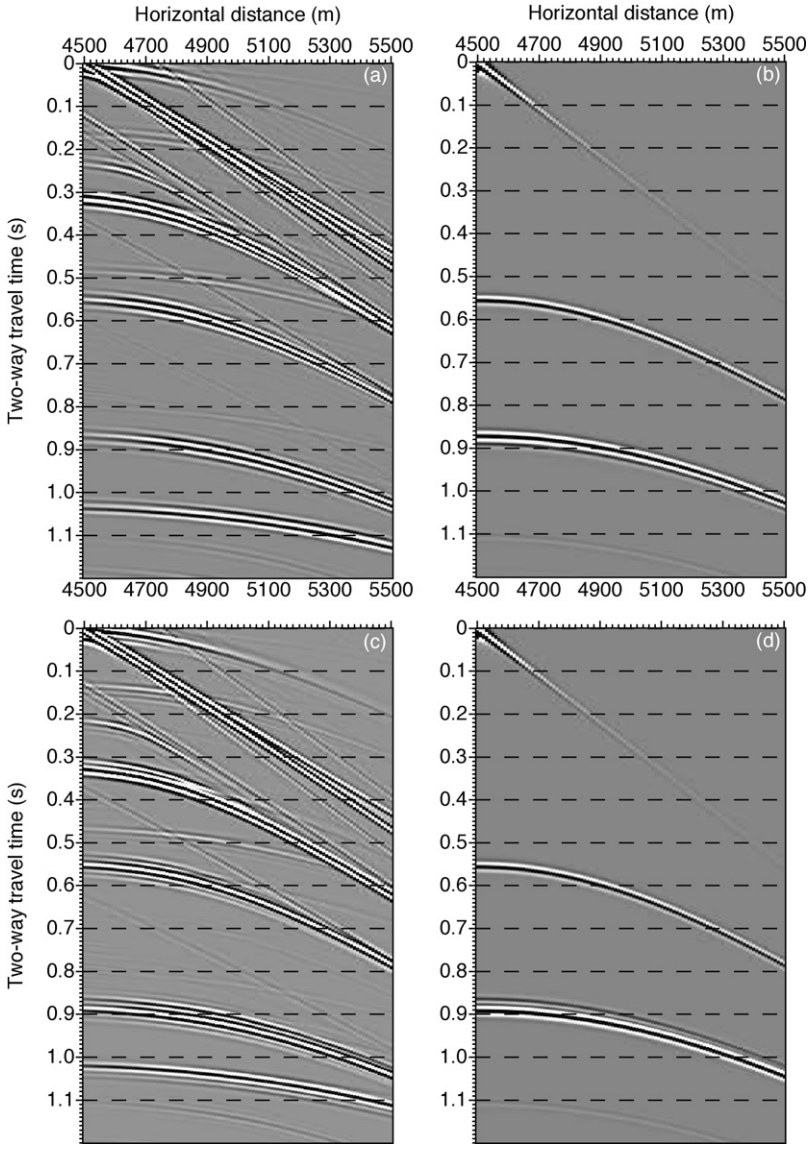


**Fig. 5.** As in Fig. 3, but for the model in Fig. 2(b).

wavelets of the ghost reflections at 0.32 s from Figs. 3(a) and 5(a)). In Fig. 5(a) we can now observe another ghost reflection with an apex at around 0.24 s. This ghost results from the correlation of the multiple reflection from the bottom of the first layer with the reflection from the bottom of the cap rock. This ghost is also present in Fig. 3(a), but is more difficult to distinguish, as it is overlain by the stronger reservoir-layer ghost.

Comparing the effective ghost reflection from inside the cap rock in Fig. 6(a) and (c) for the base and the monitor survey, respectively, with directly modelled reflections for these surveys as shown in Fig. 6(b) and (d), we can see that the effective reflection from the cap rock has been kinematically correctly retrieved for both the base and the monitor surveys. This means that the effective ghost can again be used for monitoring changes in the reservoir. Just like in the thick-reservoir case, here also the source non-repeatability does not affect the retrieval of the effective ghost reflection, see Fig. 6(e).

### 3.2. Laboratory tests

We test the applicability of the above method through scaled laboratory experiments. For this, we use a two-layer sample consisting of a top layer of epoxy, representing a cap rock, and a lower layer of Bentheimer sandstone, representing the reservoir rock (Fig. 7). The sandstone has a porosity of 21.7%, permeability of 1.34 D ($1.34E^{-12}$ m$^2$) and density of 2080 kg/m$^3$. We make use of 1 MHz P-wave transducers from Panametrics as sources and receivers. The transducers are directly glued to the surface of the sample using an acoustic couplant. The source transducers are fed with a sine-wave signal from an Agilent 33210A function generator, the signal is afterwards amplified by 50 dB by means of an ENI 2100L RF amplifier. The measured signal is quality-controlled with a Yokogawa DL4200 oscilloscope and then stored on a PC. For a first series of measurements we use two receivers, R1 and R2, placed on the epoxy and spaced 30 mm from each other. Sources are placed at multiple positions to the left of the receivers. Our recording geometry mimics a marine-survey acquisition geometry. The first source is at 18.5 mm offset from receiver R1. After one measurement, the source is moved to the left by approximately, but not exactly, 2.5 mm and a new measurement is made. The left-most position of the receiver has an offset of approximately 56 mm from receiver R1. Using this scheme, we make four measurements. First, we measure the reflection responses for all source positions when the sandstone is saturated with brine. After that, we measure the reflection response for all source for cases when the brine is being

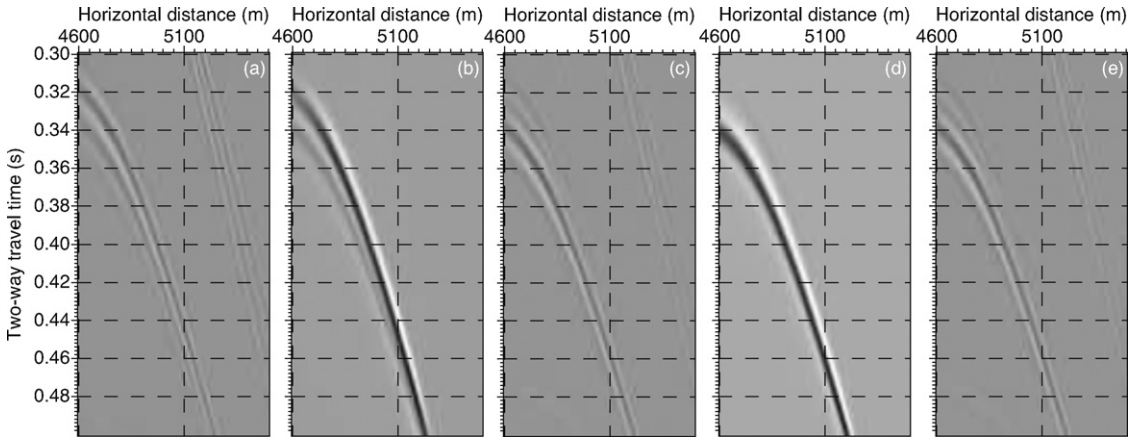


**Fig. 6.** As in Fig. 4, but for the model in Fig. 2(b).

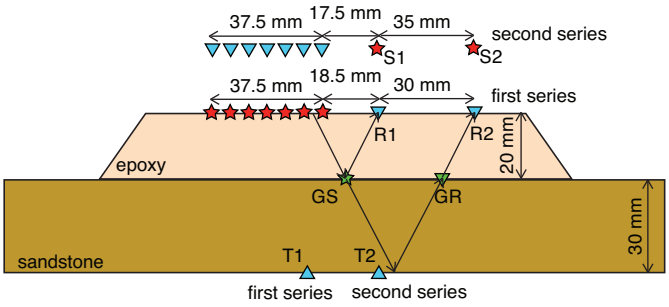


**Fig. 7.** Cartoon of the scaled laboratory experiment. The sample consists of two layers: an epoxy plate at the top, representing a cap rock, and a plate of Bentheimer sandstone, representing a reservoir rock. The red stars (e.g. S1 and S2) indicate the locations of 1 MHz P-wave source transducers; the blue triangles (e.g. R1, R2, T1 and T2) represent 1 MHz P-wave receiver transducers; the green star and triangle represent, respectively, the locations of the ghost source GS and the ghost receiver GR. Two series of measurements are performed. During the first one, we used R1, R2, T1 and the array of sources (red stars). During the second series of measurements, we use S1, S2, T2 and the array of receivers (blue triangles).

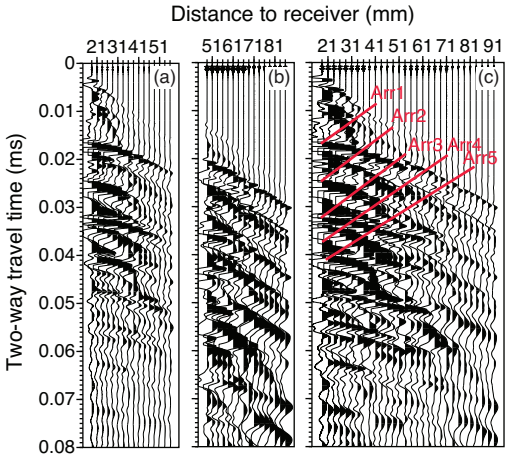


**Fig. 8.** Recorded reflection common-receiver gather when brine is displaced after injecting ethanol equal to about the total amount of the calculated pore volume of the sandstone for (a) receiver R1 and (b) receiver R2. (c) A combined reflection common-receiver gather obtained by concatenating the recordings from the panel in (a) up to source-receiver offset of 46 mm and the complete panel in (b). The red lines indicate five arrivals, labelled Arr1 to Arr5.

displaced by ethanol. The measurements are done after injecting ethanol equal to about 1/3, 2/3 and the total amount of the calculated pore volume of the sandstone. As ethanol dissolves in water, we are not sure how much brine is really displaced.

Fig. 8(a, b) show the common-receiver gathers recorded at receiver R1 and R2, respectively, after injecting ethanol equal to about the total amount of the calculated pore volume. To make the interpretation of the recorded events easier, we combine the two common-receiver gathers into one supergather, where the offsets up to 46 mm are taken from the gather in Fig. 8(a), while the offsets of 48.5 mm and longer are taken from the gather in Fig. 8(b), see Fig. 8(c). In the latter figure, the arrival marked Arr1 is the P-wave reflected from the top of the sandstone; Arr2 is the converted reflection from the top of the sandstone, where one of the legs is traversed by a P-wave and the other by an S-wave; Arr3 is the first multiple of Arr1; Arr4 is the S-wave reflection from the top of the sandstone; Arr5 is the reflection from the bottom of the sandstone. Note that the reflection hyperbolae are a bit irregular along their curvature, as a result of the approximately, but not exactly, 2.5 mm source interval. This irregularity realistically mimics the non-repeatability of the source positions in field seismic surveys.

With these four measurements, we try to follow different stages of injection of $CO_2$ inside the reservoir. As the Utsira formation in the Sleipner field is at 800 m depth, the injected $CO_2$ will be in a supercritical condition (Arts et al., 2002, 2008). To use a sample with injected supercritical $CO_2$ in it, a special setup that can withstand high pressures is required. To avoid this for the time being, we opt to use ethanol instead of supercritical $CO_2$. Ethanol has the advantage of being easy to handle under room conditions, while its seismic characteristics are at an intermediate level between water and supercritical $CO_2$, see Table 1. If our approach proves to be capable of monitoring brine replacement by ethanol, then we expect an even better performance in the case of brine replacement by supercritical $CO_2$, as the velocity change is much larger for the latter case.

**Table 1**
Seismic properties of water, ethanol and supercritical $CO_2$. The properties of water and ethanol are calculated for temperature of 25 °C and 0.1 MPa, while for supercritical $CO_2$ – at 32 °C and 10 MPa.

| Substance | P-wave velocity (m/s) | Density (kg/m$^3$) | Isothermal bulk modulus (MPa) |
|---|---|---|---|
| Water | 1496.3 | 997.09 | 2209.3 |
| Ethanol | 1139.4 | 785.60 | 868.83 |
| Supercritical $CO_2$ | 363.01 | 751.67 | 27.629 |

After all the measurements are performed, we apply SI Eq. (1) to the measured seismic reflection common-receiver gathers.

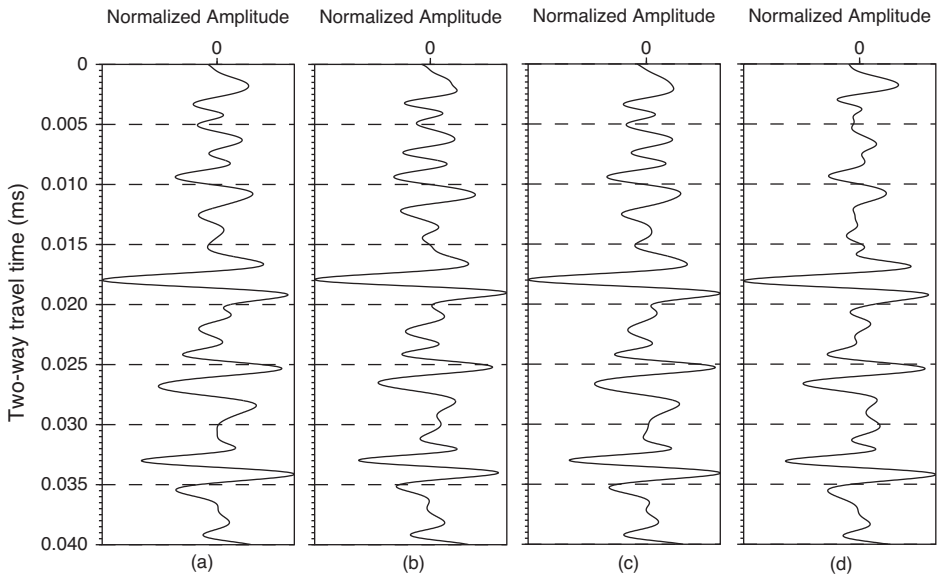


**Fig. 9.** Causal part of the retrieved seismic-interferometry results, as would be recorded by receiver at R2 as if there were a virtual source at R1. The virtual measurements are performed when the sandstone reservoir (a) is saturated with brine and when the brine is displaced by injecting ethanol equal to about (b) 1/3, (c) 2/3 and (d) the total amount of the calculated pore volume.

We correlate the gather at R1, representing $G(\mathbf{x}_A, \mathbf{x}, t)$, with the gather at R2, representing $G(\mathbf{x}_B, \mathbf{x}, t)$. The result represents the integrand in Eq. (1). After that, we sum the correlation results over the source positions $\mathbf{x}$ to obtain the left-hand side of Eq. (1). Because the sources are to the left of the receivers, the SI result contains retrieved physical events only in its causal part ($t \geq 0$ s), so as a final retrieved result we look only at the causal part. This procedure is repeated for the other three measurements as well. The resulting reflection traces as would be observed at R2 due to a virtual source at R1 are shown in Fig. 9(a–d). In all four traces, we can see an event at 0.018 ms. This event represents the retrieved reflection from the bottom of the epoxy cap rock. When applying Eq. (1) to the recorded common-receiver gathers, this event is retrieved from the correlation of Arr1 with Arr3. Following the arrival time of this reflection on the four traces when the brine inside the reservoir is being displaced by the ethanol, we see that there is no change in the arrival time. Thus, as expected, no changes have taken place in the cap rock.

In Fig. 9(a) we can also see an event at 0.0267 ms. When applying Eq. (1) to the recorded common-receiver gathers, this event results from the correlation of Arr1 with Arr5. The event represents the ghost reflection from inside the sandstone reservoir as if a ghost source and a receiver have been placed directly on top of the sandstone. The two-way travel time of the ghost does show small changes during the brine displacement. Fig. 10(a–d) shows a zoomed-in version (between 0.023 ms and 0.03 ms) of the respective traces shown in Fig. 9(a–d). Now we can clearly distinguish that the strongest negative peak indicates a change in the arrival time of the ghost reflection when the brine in the reservoir is displaced by ethanol. When ethanol amounting to about 1/3 of the pore volume is injected, the ghost reflection arrives 0.0004 ms earlier; for injection of ethanol in the reservoir of about 2/3 and the total amount of the pore volume, the ghost reflection arrives only 0.0002 ms earlier.

Because the sample is composed of horizontal layers and the cap layer of epoxy is assumed to be laterally homogeneous, the distance between the ghost virtual source and receiver is equal to the distance between the virtual source and receiver at the top of the cap rock, i.e. is equal to 30 mm. Knowing the ghost source-receiver offset for each of the obtained ghost reflections, we can calculate the P-wave velocity inside the reservoir. We calculate for the brine-saturated sandstone a P-wave velocity of 2503 m/s, for the case of injected ethanol amounting to about 1/3 of the pore volume – 2541 m/s, while for the case of injected 2/3 and the total volume – 2522 m/s.

By applying Eq. (1) to the full common-receiver gathers in Fig. 8(a, b) we would retrieve the complete Green's function when the surface-source distribution allows it. In our case, the result contains the physical reflection from the top of the reservoir and the ghost reflection from inside the reservoir, but also other (non)physical events, see Fig. 9. For example, the retrieved arrival at 0.011 ms is a non-physical one and results from the correlation of Arr1 and Arr2. The result from the correlation and summation in the SI equation might give rise to a physical or a non-physical event that might overlay partly or completely the reflection ghost from the reservoir and thus influence the estimation of the reservoir velocities. This can be avoided by choosing which parts of the common-receiver gathers in Fig. 8(a, b) we "feed" in Eq. (1). Using the interpretation regarding which recorded reflection arrivals cause the retrieval of the ghost reflection in Fig. 9(a–d), we choose to "feed" to Eq. (1) only the reflections from the bottom of the epoxy and the bottom of the sandstone. That is, from the common-receiver gather in Fig. 8(a) we keep only arrivals Arr1, while from the gather in Fig. 8(b) we keep only arrival Arr5; all other events are muted. These pre-processed gathers are cross-correlated and the result is summed along the surface sources (application of Eq. (1)). The results, zoomed in around the time of the retrieved ghost reflection, are shown in Fig. 11. Following the strongest negative peak, we see that the change in the arrival time of the reflection ghost exhibits the same trend as in Fig. 10, but the arrival times and travel time changes are a bit different. Compared to the arrival time of the ghost for a brine-saturated sample, when ethanol amounting to about 1/3 of the pore volume is injected, the ghost reflection arrives 0.00025 ms earlier; for injection of ethanol amounting to about 2/3, the ghost arrives 0.00015 ms earlier; and for injecting the total amount of the calculated pore volume, the ghost reflection arrives only 0.0001 ms earlier. For the arrival times in the figure, we calculate for the brine-saturated reservoir a velocity of 2521 m/s, for the case of injected ethanol amounting to about 1/3 of the pore volume – 2545 m/s, for the case of injected 2/3 – 2536 m/s, and for the case of injecting the total amount of the calculated pore volume – 2531 m/s.

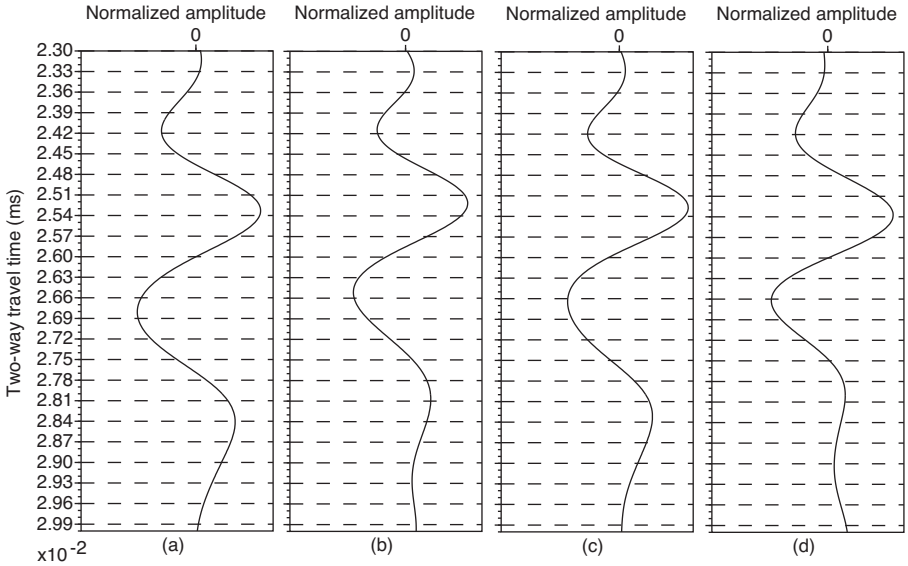


**Fig. 10.** As in Fig. 9, but zoomed-in between 0.023 ms and 0.03 ms.

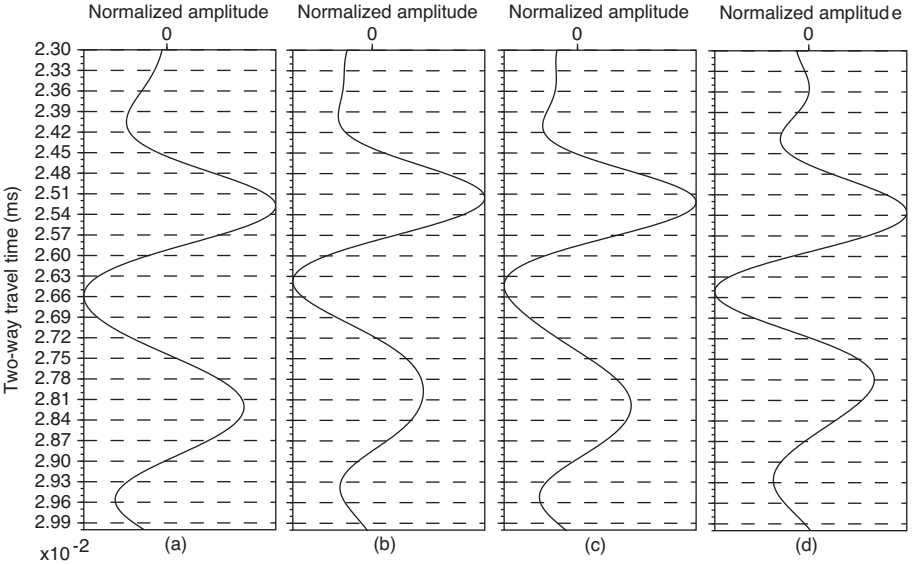


**Fig. 11.** As in Fig. 10, but when only Arr1 and Arr5 from Fig. 8(a) and (b), respectively, are used in the seismic-interferometry retrieval procedure.

Using the above velocities, we calculate that the stationary-phase point for a retrieved reflection between a virtual source at R1 and a receiver at R2 is at 22.5 mm to the left of R1. This means that to the right of the stationary-phase point there are only two sources contributing to the constructive or destructive summation along the sources in the application of Eq. (1), while to the left of the stationary-phase point there are more sources. The very limited number of sources to the right of the stationary point might result in an erroneous retrieved wavelet of the ghost reflection and thus also influences the velocity estimation.

To estimate independently the propagation velocities inside the sandstone reservoir during the brine-displacement process, we measure also the transmission response across the sample using a receiver transducer T1 positioned as shown in Fig. 7. We make use of the arrival times of the direct P-wave. The estimated velocities show the same trend change as in Fig. 10, but the values are different. Due to the source non-repeatability introduced purposefully by us during the recording of the four datasets, the positioning of T1 with respect to the source (which should be vertically above it) is not exact. This might have resulted in errors in the estimation of the velocities.

To avoid the non-repeatability problem with the transmission measurements in the first series of measurements, we perform a second series of measurements, see Fig. 7. Making use of source-receiver reciprocity, we use fixed sources at S1 and S2 and an array of receivers (blue triangles in Fig. 7). We also place at the bottom of the sandstone a transducer at T2 for recording transmission arrivals; T2 is located precisely vertically below the position of S1. We measure in a way similar to that for the first series of measurements – we place a reflection transducer at the top of the epoxy at a certain position and record at that position and at T2 the arrivals from the two sources at S1 and S2. After that the reflection receiver is moved to the left by approximately, but not exactly, 2.5 mm and new recordings from S1 and S2 are made. As for the first series, we carry out measurements for four cases of reservoir fluids: when the reservoir is saturated with brine and when the brine is displaced

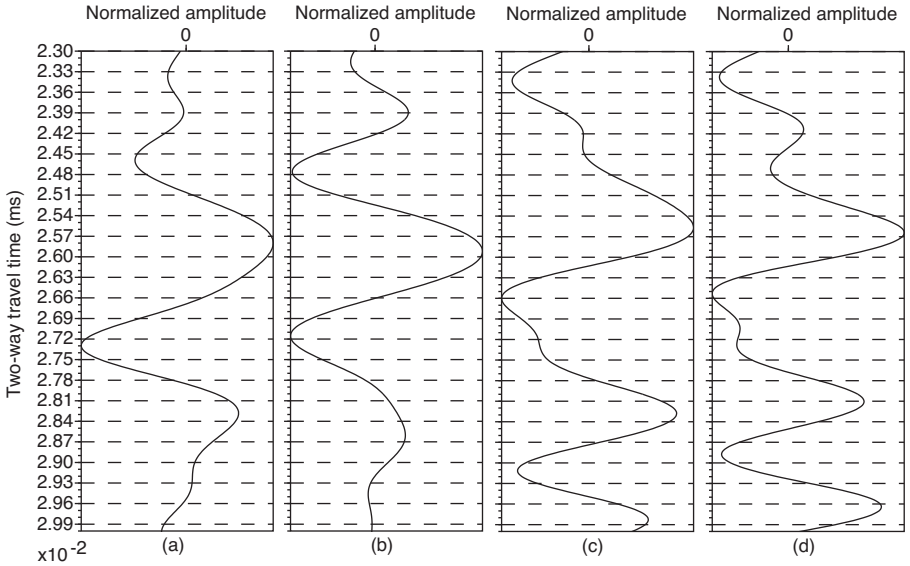


**Fig. 12.** As in Fig. 11, but for the second-series measurements.

by injection of ethanol amounting to 1/3, 2/3, and the total amount of the estimated pore volume.

Aiming to have more sources also to the left of the stationary-phase point, for the second series of measurements we separate S1 and S2 by 35 mm and place the first receiver at a distance of 17.5 mm to the left of S1. Using the estimated velocities from the first series of measurements, we calculate that the stationary-phase point for the new geometry will be for a receiver at 26.5 mm to the left of S1. Thus, this acquisition geometry would help to have a better retrieval of the wavelet of the ghost reflection from inside the reservoir.

Application of SI to the second series of measurements would retrieve the reflection response as would be observed by a receiver at S2 due to a virtual source at S1. From the first series of measurements we know how to interpret the newly recorded reflection arrivals. For this reason, we directly apply Eq. (1) only to the newly recorded Arr1 measured using S1 and to the newly recorded Arr5 measured using S2; the rest of the recorded arrivals are again muted. The results are shown in Fig. 12. Following the strongest negative peak, we see that, when ethanol is being injected, the propagation velocity of the P-waves inside the reservoir again increases: from the brine-saturated condition of 2544 m/s, the velocity slightly increases to 2558 m/s when injecting ethanol amounting to about 1/3 of the calculated pore volume, and then increases even further to 2611 m/s and 2616 m/s, when injecting 2/3 and the total amount of the calculated pore volume, respectively.

Fig. 13(a–d) shows, for the four cases of reservoir liquid, the first P-waves arrivals recorded at T2 from the source at S1. Following the strongest positive peak, we can see that when the brine inside the sandstone is being displaced by injected ethanol, the velocity of the P-waves increases. This is a trend similar to the one in Fig. 12(a–d). However, the changes in the arrival times are a bit different. As the cap rock does not change during the experiment, changes in the arrival times should be indicative of changes in the velocity inside the reservoir. The P-waves velocity inside the

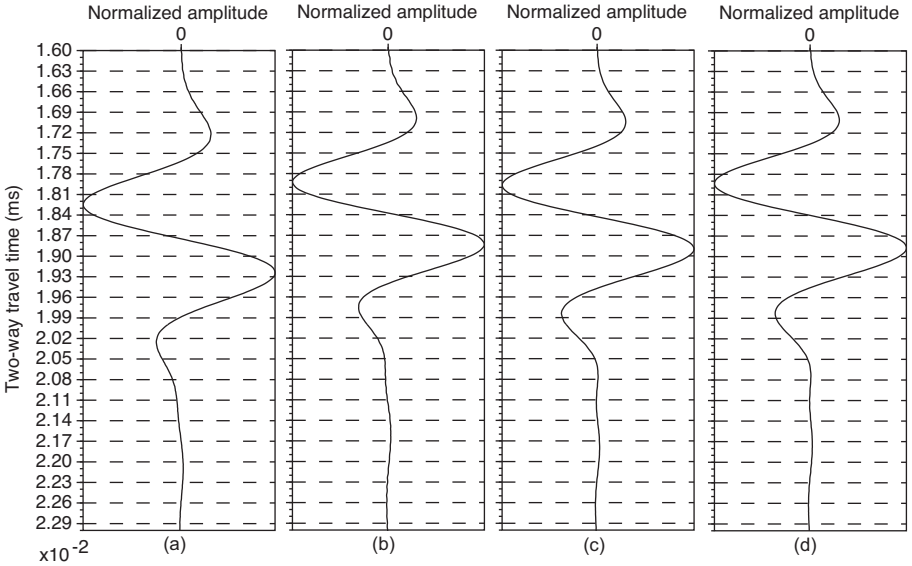


**Fig. 13.** Recorded first arrivals of the transmission response when the sandstone is saturated with (a) 100% brine and when brine has been displaced by injecting ethanol equal to about (b) 1/3, (c) 2/3 and (d) the total amount of the calculated pore volume.

**Table 2**
Estimated P-wave velocity (in m/s) inside the sandstone reservoir when (from left to right) it is saturated with brine and when ethanol equal to about 1/3, 2/3 and the total amount of the calculated pore volume is injected, respectively.

| Sample experiment | Brine-saturated | Ethanol of 1/3 injected | Ethanol of 2/3 injected | Ethanol of total pore volume injected |
|---|---|---|---|---|
| Transmission | 2520 | 2607 | 2594 | 2596 |
| Ghost reflection | 2544 | 2558 | 2611 | 2616 |

epoxy is obtained using S1 and T2 on the sample before saturating it with brine. Using the thickness of the cap rock and the arrival-time difference between the first arrival and its multiple, which has reflected inside the epoxy layer, we calculate 2727 m/s for the velocity inside the epoxy. Using this value, together with the thickness values of the cap rock and the reservoir, we calculate for the brine-saturated sandstone a velocity of 2520 m/s, for the case when ethanol amounting to about 1/3 of the estimated pore volume is injected – 2607 m/s, for the case when ethanol amounting to about 2/3 is injected – 2594 m/s, and when the total amount is injected – 2596 m/s.

## 4. Discussion

The results from the laboratory tests show that ghost reflections retrieved by application of SI to surface reflection data can be used to monitor displacement of fluids in a $CO_2$ reservoir, see Table 2. We observe that when brine is being displaced by ethanol, the velocity of the resulting fluid has increased. However, the quantitative description of the velocity changes that takes place differs a bit from the one obtained from direct transmission measurements. For the case when the sandstone reservoir is saturated with brine the difference between the velocity estimated from the transmission and the reflection-ghost measurements is 0.95%; for the cases when ethanol of about 2/3 and the total amount of the calculated pore volume is injected the differences are even smaller – 0.66% and 0.77%, respectively. When ethanol of about 1/3 of the calculated pore volume is injected, the difference in the estimated velocities is a bit bigger – 1.88%. The differences are quite small and might be due to the development of preferred paths for migration of brine and ethanol inside the reservoir. This process affects in different ways the reflection and the transmission measurements, as the corresponding transducers are placed at different locations along the length of the sample. The transmission transducer is placed vertically below the transducer at S1. On the other hand, the ghost source and receiver would measure the reflection from inside the reservoir from a reflection point at the bottom of the sandstone which is to the left of the line S1T1. We calculate the stationary-phase point, but this time using the transmission velocities from Table 2, and find it to be at 26.5 mm and 25 mm to the left of S1T1 for the brine-saturated reservoir and after injection of ethanol equal to the total amount of the calculated pore volume. For these values, the reflection point from the bottom of the reservoir for the ghost reflection is at 13.25 mm and 12.5 mm, respectively, from the line S1T1. Another factor that needs to be considered when comparing the values estimated from the transmission and the reflection-ghost measurements is that the transmission ray passes through the reservoir only along one path, while the reflection-ghost ray passes the reservoir along two lines. The latter might result in averaging of the sampled velocities along two location with different preferred paths for migration of brine and ethanol inside the reservoir.

In our experiments, we displace the brine by injecting ethanol equal to about 1/3, 2/3 and the total amount of the calculated pore volume of the sandstone layer. In the previous subsection, we mention that we are not sure how much brine is effectively displaced, because the two liquids mix well. To try to make an estimation of the displaced brine, we calculate the expected P-wave velocities. In our laboratory experiment, we make use of ultrasonic frequencies. For such frequencies, the saturated-rock seismic parameters will most likely not be described well by the Gassmann's relations (Mavko et al., 2009, pp. 281–282). Because of this, we use Biot's theory to calculate the high-frequency limit of the P-wave velocity for a sandstone saturated with brine and with ethanol. The obtained values are 2837 m/s and 2620 m/s, respectively (Mavko et al., 2009, p. 267). The fact that the measured velocities are lower, might mean that we need to use wetted-frame moduli in the velocity calculation with Biot's theory (Bacri and Salin, 1986). Nevertheless, we can use the theoretically calculated velocities for qualitative interpretation. We see that a sandstone saturated with ethanol should exhibit a lower velocity than a sandstone saturated with brine. Comparing the values in the left-most column in Table 2 with those in the right-most column of the estimated velocities, we see that when ethanol of about the total amount of the calculated pore volume is injected in the sandstone reservoir the estimated velocity is higher than that for the sandstone saturated with brine. Resa et al. (2005, 2009, Table 3 and Fig. 3, respectively) and Vatandas et al. (2007, Fig. 3) performed ultrasonic measurements of the binary mixture water–ethanol, and reported that when the ethanol concentration in the water is low, the measured P-wave velocity is higher than that for pure water. The measured velocity reaches maximum at an ethanol concentration of about 20% and is with about 100 m/s higher than the velocity in pure water. When the ethanol concentration is increased above this value, the measured velocity of the mixture decreases and for about 50% ethanol the velocity is about 50 m/s lower than that in pure water. Using these observations, we might interpret the estimated velocities to be indicating that even after injecting ethanol equal to about the total amount of the calculated pore volume, the displaced brine is only about 20% (at least at the points of observation of the ghost reflections and transducer T2).

As shown with the numerical and laboratory data, the ghost reflections obtained from SI are sensitive to velocity changes only inside the layer that caused them to appear in the SI result, for example only inside the $CO_2$ reservoir or in the cap rock. This is an important advantage of this method compared with the velocity analysis in standard reflection-data processing. In the latter, an error in the estimation of the velocity in the layers above the reservoir will be propagated in the estimation of the velocity inside the reservoir.

The results we show are obtained for a horizontally layered medium. When the subsurface is not horizontally layered, the ghost reflections can still be used for qualitatively monitoring the displacement inside the $CO_2$ reservoir, but the exact quantitative interpretation will be hampered, because the distance between the ghost source and receiver will not be known exactly. If a borehole instrumented with geophones is available, then application of SI to data measured inside the borehole from surface seismic sources will again retrieve the layer-specific reflection ghosts (Draganov et al., submitted for publication). The latter can be used for precise monitoring of velocity changes inside the reservoir at the point where the borehole crosses the reservoir. This can complement the qualitative results from the method we showed here, which will indicate the displacement in the lateral direction.

## 5. Conclusions

We have proposed the use of non-physical (ghost) arrivals retrieved from the application of seismic interferometry to surface reflection seismic data for monitoring changes in $CO_2$ reservoirs. These ghosts represent reflection arrivals from inside separate subsurface layers as if measured with sources and receivers directly placed on the top of each of these layers. Using numerical dataset from a horizontally layered model, that can be considered representative for a Sleipner type of $CO_2$ storage reservoir in the North Sea, we have shown that the ghost reflections capture layer-specific changes in the reservoir velocity that have occurred between a base and a monitor survey. Next, we have tested the method on data from a scaled laboratory experiment with 1 MHz P-wave transducers. The laboratory sample consists of an epoxy plate, representing a cap rock, placed on a plate of Bentheimer sandstone, representing a reservoir layer. We have simulated displacement of brine by $CO_2$. In the Sleipner field the $CO_2$ is in a supercritical condition. For ease of handling the sample in room conditions, we have used ethanol instead of supercritical $CO_2$; the values of the seismic characteristics of the ethanol are between those of water and supercritical $CO_2$. Using the retrieved ghost reflection from inside the reservoir, we have found that when the brine is displaced by ethanol, the velocity in the reservoir increases. We have observed the same trend using direct transmission measurements. We interpreted this trend to be an indication for about 20% brine displacement.

## References


Arts, R., Chadwick, A., Eiken, O., Thibeau, S., Nooner, S., 2008. Ten years' experience of monitoring $CO_2$ injection in the Utsira and at Sleipner, offshore Norway. First Break 26, 65–72.

Arts, R., Eiken, O., Chadwick, A., Zweigel, P., van der Meer, L., Zinszner, B., 2004. Monitoring of $CO_2$ injected at sleipner using time-lapse seismic data. Energy 29, 1383–1392.

Arts, R., Elsayed, R., van der Meer, L., Eiken, O., Ostmo, S., Chadwick, A., Kirby, G., Zinszner, B.,2002. Estimation of the mass of injected $CO_2$ at Sleipner using time-lapse seismic data. In: 64th Conference and Exhibition Extended Abstracts. EAGE, p. H16.

Bacri, J.-C., Salin, D., 1986. Sound velocity of a sandstone saturated with oil and brine at different concentrations. Geophysical Research Letters 13, 326–328.

Bharadwaj, P., Schuster, G., Mallinson, I., Dai, W., 2011. Theory of supervirtual refraction interferometry. Geophysical Journal International, published online.

Campillo, M., Paul, A., 2003. Long-range correlations in the diffuse seismic coda. Science 299, 547–549.

Carcione, J.M., Picotti, S., Gei, D., Rossi, G., 2006. Physics and seismic modeling for monitoring $CO_2$ storage. Pure and Applied Geophysics 163, 175–207.

Chadwick, A., Williams, G., Delepine, N., Clochard, V., Labat, K., Sturton, S., Buddensiek, M.-L., Dillen, M., Nickel, M., Lima, A.L., Arts, R., Neele, F., Rossi, G., 2010. Quantitative analysis of time-lapse seismic monitoring data at the Sleipner $CO_2$ storage operation. The Leading Edge 29, 170–177.

Claerbout, J.F., 1968. Synthesis of a layered medium from its acoustic transmission response. Geophysics 33, 264–269.

Curtis, A.D.H., 2010. Source-receiver wave field interferometry. Physical Review E 81, 046601.

Dong, S., Sheng, J., Schuster, G.,2006. Theory and practice of refraction interferometry. In: 76th Annual International Meeting Expanded Abstracts. SEG, pp. 3021–3025.

Draganov, D., Ghose, R., Heller, K., Ruigrok, E., Monitoring of changes in velocity and Q in reservoirs using non-physical arrivals in seismic interferometry. Geophysical Journal International, submitted for publication.

Draganov, D., Ghose, R., Ruigrok, E., Thorbecke, J., Wapenaar, K., 2010. Seismic interferometry, intrinsic losses and Q-estimation. Geophysical Prospecting 58, 361–373.

Ivanova, A., Kashubin, A., Juhojuntti, N., Kummerow, J., Henninges, J., Juhlin, C., Lüth, S., Ivandic, M., Monitoring and volumetric estimation of injected $CO_2$ using 4D seismic, petrophysical data, core measurements and well logging: a case study at Ketzin, Germany. Geophysical Prospecting, published online, doi:10.1111/j.1365-2478.2012.01045.x.

Kallweit, R.S., Wood, L.C., 1982. The limits of resolution of zero-phase wavelets. Geophysics 47, 1035–1046.

King, S., Curtis, A., 2012. Suppressing nonphysical reflections in Green's function estimates using source-receiver interferometry. Geophysics 77, Q15–Q25.

King, S., Curtis, A., Poole, T.L., 2011. Interferometric velocity analysis using physical and nonphysical energy. Geophysics 76, SA35–SA49.

Lumley, D., 2010. 4D seismic monitoring of $CO_2$ sequestration. The Leading Edge 29, 150–155.

Mavko, G., Mukerji, T., Dvorkin, J., 2009. The Rock Physics Handbook, 2nd edition. Cambridge.

Mikesell, T.D., van Wijk, K., Calvert, A., Haney, M., 2009. The virtual refraction: useful spurious energy in seismic interferometry. Geophysics 74, A13–A17.

Nichols, J., Mikesell, D., van Wijk, K., 2011. Application of the virtual refraction to near-surface characterization at the boise hydrogeophysical research site. Geophysical Prospecting 58, 1011–1022.

Resa, P., Elvira, L., de Espinosa, F.M., Gómez-Ullate, Y., 2005. Ultrasonic velocity in water–ethanol–sucrose mixtures during alcoholic fermentation. Ultrasonics 43, 247–252.

Resa, P., Elvira, L., de Espinosa, F.M., González, R., Barcenilla, J., 2009. On-line ultrasonic velocity monitoring of alcoholic fermentation kinetics. Bioprocess and Biosystems Engineering 32, 321–331.

Schuster, G.T.,2001. Theory of daylight/interferometric imaging: tutorial. In: 63rd Conference and Exhibition Extended Abstracts. EAGE, p. A-32.

Schuster, G.T., 2009. Seismic Interferometry. Cambridge.

Shapiro, N.M., Campillo, M., 2004. Emergence of broadband Rayleigh waves from correlations of the ambient seismic noise. Geophysical Research Letters 31, L07614.

Snieder, R., 2004. Extracting the Green's function from the correlation of coda waves: a derivation based on stationary phase. Physical Review E 69, 046610.

Snieder, R., Wapenaar, K., Larner, K., 2006. Spurious multiples in seismic interferometry of primaries. Geophysics 71, SI111–SI124.

Tatanova, M., Bakulin, A., Mehta, K., Korneev, V., Kashtan, B.,2008. Reconstructing head waves with virtual source method. In: 78th Annual International Meeting Expanded Abstracts. SEG, pp. 183–187.

Tatanova, M., Mehta, K., Kashtan, B.,2011. Virtual refraction tomography: application to realistic 3D model. In: 81st Annual International Meeting Expanded Abstracts. SEG, pp. 4239–4243.

Thorbecke, J., Draganov, D., 2011. Finite-difference modeling for seismic interferometry. Geophysics 76, H1–H18.

van Wijk, K., 2006. On estimating the impulse response between receivers in a controlled ultrasonic experiment. Geophysics 71, SI79–SI84.

Vatandas, M., Koc, A.B., Koc, C., 2007. Ultrasonic velocity measurements in ethanol–water and methanol–water mixtures. European Food Research and Technology 225, 525–532.

Wapenaar, K., 2006. Green's function retrieval by cross-correlation in case of one-sided illumination. Geophysical Research Letters 33, L19304.

Wapenaar, K., Draganov, D., Robertsson, J.O.A. (Eds.), 2008. Seismic Interferometry: History and Present Status. Vol. 26 of Geophysics Reprint Series. SEG, Tulsa, OK.

Wapenaar, K., Fokkema, J., 2006. Green's functions representations for seismic interferometry. Geophysics 71, SI33–SI46.

Wapenaar, K., Thorbecke, J., Draganov, D., Fokkema, J.,2002. Theory of acoustic daylight imaging revisited. In: 72nd Annual International Meeting Expanded Abstracts. SEG, p. ST 1.5.